

Outlook on Bering Sea Oxygen Cycling:
Regional Ocean Simulations of Future Change

Samuel Mogen
Radford, VA

A Thesis presented to the Faculty
of the University of Virginia
in Fulfillment of the
Distinguished Majors Program

Department of Environmental Sciences
April 2020

Scott C. Doney,
Thesis Advisor

Thomas M. Smith,
Director of Distinguished Major Program

Abstract

Estimates suggest that the global ocean oxygen inventory has declined by ~2% since the mid-20th century. Strong signals of decline in dissolved oxygen have been detected in the Gulf of Alaska and subpolar North Pacific. The adjacent Bering Sea region supplies ~60% of U.S. fish catch by weight annually and any environmental changes to the region threaten the U.S. Blue Economy. The region is known to be affected by rapid temperature rise and ocean acidification, but few studies have examined regional oxygen decline. In this study, a regional ocean model (Bering10k) simulated oxygen cycling in the Bering Sea over past (2003-2012) and future (2006-2100) timeframes. It was expected that oxygen would decline over the 21st century and low oxygen regions would expand spatially. Bering10k hindcast and projection oxygen were validated against observed data ($R = 0.75$). Future simulations were forced using atmospheric and ocean boundary conditions derived from ensemble members of the CMIP5 archive (CESM, GFDL, MIROC) for two emission scenarios (RCP 4.5, 8.5). Long term trends suggested significant change in bottom oxygen levels on the Bering shelf by the end of the 21st century. These changes were spatially and simulation dependent, with the largest region-wide declines observed in CESM simulations (-6%). Seasonal oxygen minimums increased in frequency in both CESM and MIROC-forced simulations by 2100. Oxygen drivers also changed, with increases in respiration, remineralization and productivity, and decline in apparent oxygen utilization. Future work should quantify simulation-specific drivers in order to determine the importance of solubility, circulation, and biological processes in regional ocean oxygen.

Acknowledgements

Many thanks to the NOAA Hollings Scholarship program for providing me with the opportunity and funding to work with NOAA scientists. Thanks to my advisors and mentors, Darren Pilcher and Jessica Cross, at PMEL in Seattle for taking me on (despite initially not seeking an intern). Their guidance has been crucial in developing this project, and my future goals as a scientist. Many thanks also to the developers of the Bering10k model (Al Herman, et al.) – this project would not exist if not for their work. Thanks to Scott Doney for guiding me through the DMP and thesis-writing process (partially via Zoom). His expertise in ocean biogeochemistry has helped me better understand my data/results and exposed me to the researchers with whom I will continue my studies.

Gratitude also to Professor Jim Galloway and the Nitrogen Working Group for getting my feet wet with research at UVA and acting as a crucial source of guidance and support throughout my time at UVA. I also want to thank Julia Stanganelli for keeping me sane these last 4 years and acting as a sounding board for all that goes on in my life – your friendship means the world to me.

Finally, thanks to Professor Thomas Smith and the Distinguished Majors Program committee for their consideration of this project.

Table of Contents

Abstract	i
Acknowledgements	ii
Table of Contents	iii
List of Figures	iv
List of Equations	v
List of Tables	vi
Introduction	1
<i>Ocean Deoxygenation</i>	1
<i>The Bering Sea</i>	2
<i>Objectives</i>	4
Methods	5
<i>Model information</i>	5
<i>Variables</i>	6
<i>Model Validation</i>	6
<i>Analysis</i>	7
Results	9
<i>Model Validation</i>	9
<i>Simulation Data</i>	9
<i>Seasonal Oxygen Cycling</i>	14
<i>Oxygen Drivers</i>	17
Discussion	20
<i>Scenario-Specific Change</i>	21
<i>Seasonal Oxygen Declines</i>	23
<i>Summary</i>	24
References	25

List of Figures

Figure 1:	Validation of Bering10k hindcast model oxygen with observations	9
Figure 2:	Time series for bottom water oxygen from all simulations across the 21 st century on the Bering Sea shelf	10
Figure 3:	Difference in bottom water oxygen between initial (2011-2020) and final (2091-2100) decades on the Bering Sea Shelf for all simulations	12
Figure 4:	Spatial map of significant differences between initial and final decades via two-sided t-test	13
Figure 5:	Difference in bottom water oxygen between initial (2031-2040) and final (2091-2100) decades on the Bering Sea Shelf for MIROC simulations	14
Figure 6:	Time series of seasonal cycling in bottom water oxygen on the Bering Sea shelf for hindcast and RCP 8.5 scenarios	14
Figure 7:	Percent of months (September, October, November) with bottom water oxygen below the threshold (140 mmol per m ³) in initial decade (2011-2020) and change in percentage months below the threshold from initial to final decade	16
Figure 8:	Percent of months (September, October, November) with bottom water oxygen below the threshold (140 mmol per m ³) in initial decade (2031-2040) on the Bering Sea shelf for MIROC simulations and change in percentage months below the threshold from initial to final decade	17
Figure 9:	Time series of bottom water temperature and apparent oxygen utilization (AOU) averaged on the Bering Sea shelf for all simulations	18
Figure 10:	Time series of depth-integrated oxygen sources (productivity) and sinks (respiration + remineralization) averaged on the Bering Sea shelf for all simulations	19

List of Equations

Equation 1:	Equation for photosynthesis and respiration, biological source and sinks of marine oxygen	2
Equation 2:	Formula used to calculate equilibrium oxygen solubility in the Bering Sea from model output temperature and salinity. Derived from Garcia and Gordon (1992)	7
Equation 3:	Formula used to calculate apparent oxygen utilization (AOU) from model oxygen and equilibrium solubility	7

List of Tables

Table 1:	Variables extracted from Bering10k output	6
Table 2:	Percentage change in bottom water oxygen in by scenario and shelf region in the Bering Sea from initial to final decade. Highlighted numbers are significant via a two-sided t-test	11

Introduction

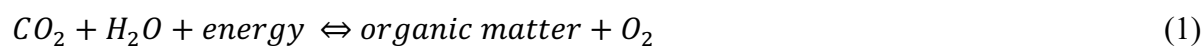
Rising atmospheric Carbon dioxide concentrations are driving global ocean temperature rise, ocean acidification, and ocean deoxygenation (Ito et al. 2015; Bopp et al. 2013). Marine temperatures play a strong role in regulating the distribution and metabolism of marine organisms such that human-driven temperature changes can interfere with ecosystems processes (Kwiatkowski et al. 2020). Since 1970, the ocean has absorbed 93% of enhanced heating due to greenhouse gases leading to regionally concentrated increases in ocean temperatures and a 0.7°C increase in global sea surface temperature (SST) since the early 20th century (Laffoley et al. 2016). The ocean has simultaneously absorbed ~30% of total anthropogenic CO₂ emissions since pre-industrial times (Khatiwala et al. 2009). Absorption of atmospheric CO₂ by the ocean results in the formation of carbonic acid, and the dissociation of this acid lowers ocean pH, driving acidification (Feely et al. 2004; Doney et al. 2009).

Ocean Deoxygenation

Long-term trends in ocean oxygen can be hard to detect due to sparse sampling, but limited observational data suggests that the global dissolved oxygen inventory has declined since the mid-20th century by 1-2%, with especially strong regional signals after the mid-1980s (Breitburg et al. 2018; Ito et al. 2015; Laffoley et al. 2019). Several investigations have noted regions with strong oxygen declines, including the Western Subpolar North Pacific and the Gulf of Alaska (Ito et al. 2015).

Global deoxygenation is considered the result of decreasing ocean oxygen solubility and increased ocean stratification, along with changes in biological processes that results from increased temperatures (Kwiatkowski et al. 2020). Global analysis of the emergence time of anthropogenic impacts within the ocean thermocline suggests that oxygen depletion emerges

more rapidly than temperature increase, likely due to changes in ocean ventilation (Hameau et al. 2020). Beyond changes in physical processes, changes in biological processes may also have a large impact on the global ocean oxygen inventory. Simultaneous changes in productivity and respiration rates can potentially mitigate or exacerbate deoxygenation (Oschlies et al. 2018). Photosynthesis and respiration are the prime biological processes affecting ocean oxygen cycling (Equation 1). In equation 1, the forward reaction refers to photosynthesis, and the reverse to respiration.



Due to the difficulty of sampling and estimating oxygen inventories at the ocean basin scale, there is precedent for using regional ocean models to estimate changes in oxygen under different climate scenarios (Siedlecki et al. 2015; Bopp et al. 2013). Earth System Model (ESM) simulations show that ocean oxygen content is sensitive to rising temperatures as they lead to decreased oxygen solubility in water, ocean stratification and decreased air-sea oxygen flux (Ito et al. 2015). Simultaneous warming and oxygen decline are projected to reduce the metabolic index (ratio of available oxygen to oxygen demand, which is also temperature dependent) for many organisms by ~50% in the northern high latitudes, forcing the poleward migration of habitats and species (Deutsch et al. 2015).

The Bering Sea

The Bering Sea is an important fishery and one of the most productive marine ecosystems in the world. The region supports a commercial fishery of over \$3 billion per year that constitutes approximately 40% of all U.S. fish landings by value (Wiese et al. 2012). Despite its economic importance, ocean biogeochemical cycling in the Bering Sea is relatively poorly understood, with little observational data due to its remote location, harsh winters and large

scale. Generally, the region is considered to have three biophysical domains: a vertically well-mixed inner shelf (0 to 50 meters), a seasonally dependent middle shelf well-mixed in the winter and stratified in the summer (50 to 100 meters), and a gradually mixed outer shelf domain (100 to 250 meters) (Hermann et al. 2019). Hydrographic surveys of the region have shown that dissolved oxygen values near the surface are high, and generally begin reaching a minimum from 100 to 400 meters depth (Talley 2007). Dissolved oxygen levels in the region are high near the surface due to cold water temperatures, frequent contact with the atmosphere, and high productivity; these levels generally decline with depth due to the strength respiratory processes (Panteleev et al. 2013). The effects of climate change and warming on this oxygen is unclear, as the wide and shallow shelf is expected to warm rapidly (Herman et al. 2019). Work was undertaken by the Bering Ecosystem Study (BEST) and Bering Sea Integrated Research Project (BSIERP) in 2008-2010 to begin modelling regional changes to ocean chemistry.

A regional biophysical model (Bering10k) was developed as a part of the BEST-BSIERP program and was used to project changes in the Bering Sea under different climate change scenarios (Hermann et al. 2016). Observational data gathered during the BEST-BSIERP program has validated the Bering10k for ocean alkalinity and pH (Pilcher et al. 2019). Regional modelling with Bering10k forced by three CMIP5 ensemble members (NOAA GFDL-ESM2M, NCAR-CESM, MIROC) for RCP 4.5 and 8.5 indicates a warming of 1-2°C between 2010 and 2040 on the Bering Sea shelf, with interannual sea-ice extent variation consistent with current variation until around 2040 followed by sea-ice decline (Hermann et al. 2016). Under high emission scenarios (RCP 8.5), Bering Sea bottom water temperatures may warm by as much as 5°C by 2100 (Hermann et al. 2019).

Objectives

This work used the Bering10k model forced by different climate scenarios (as in Herman et al. 2019) to determine the future of oxygen cycling and bottom water O₂ values in the Bering Sea. Focus was placed on oxygen thresholds at the median sublethal oxygen concentration (~140 mmol O₂ per m³) for generic fish populations (Vaquer-Sunyer and Duarte, 2008). This threshold was chosen as it results in fish mortality alongside physiological and behavioral changes that may affect fisheries. It was hypothesized that oxygen levels would significantly decrease over the 21st century across the Bering Sea shelf. Seasonal periods and regional zones meeting the low oxygen threshold were expected to become more common and widespread by 2100. The strength of oxygen decline was also expected to be largest under high emission scenarios (RCP 8.5) for each simulation.

Methods

Model information

The Bering10K model is a regional biophysical model based on the Regional Ocean Modeling System (ROMS) version 3.2, developed as part of the Bering Ecosystem Study and Bering Sea Integrated Research Project (as described in Herman et al. 2013). The Bering10k was gridded at 10km horizontal resolution, with ten vertical levels. Bathymetry was derived from ETOPO5 and smoothed for stability. Bering10K simulates both sea-ice and tidal mixing based on climatological values derived from global models. Winds, temperature, relative humidity, radiation and model SST were used to calculate surface stress, net transfer of sensible heat, latent heat, shortwave, and longwave radiations through bulk forcing flux equations. The lower trophic level biological dynamics (Nutrient, Phytoplankton, Zooplankton, NPZ) model includes two size categories for phytoplankton and sea-ice plankton, and distinguishes microzooplankton, copepods, *Neocalanus*, and Euphausiids (including krill). Metabolic conditions are temperature-dependent, leading to different food web structure in cold or warm conditions. Within the model, respiration refers to respiration of the zooplankton group and remineralization refers to detrital remineralization, so the sum of respiration and remineralization reflects the community biological oxygen demand. Further details of physical and biological model properties and tuning are provided in Herman et al. (2016 and 2019).

A hindcast model simulation in Bering10k from 2003-2012 used climatological and ocean boundary conditions derived from that period. Global simulations from CMIP5 spanning the range of model type and future human actions (NOAA GFDL-ESM2M, NCAR-CESM, MIROC) under different emission scenarios (RCP 4.5 and RCP 8.5) were downscaled and forced model simulations from 2006-2100 (note: CESM at RCP 4.5 runs only through 2079). Biological

initial conditions were derived from present climatology, and simulations were forced with boundary conditions derived from each year of global simulations (2006-2100). Model output from hindcast and future projection simulations were re-gridded from the native model grid to a 1.0 degree longitude by 0.5 degrees latitude grid in the Bering Sea region, bounded by 180W-150W and 52N-66N, and 29 uniform depths levels (from the original depth-following sigma coordinate of ROMS).

Variables

Several variables from Bering10k output were extracted from the model output to be analyzed across the spatial region and time period (Table 1). These were chosen to provide information on drivers of oxygen cycling.

Table 1: Variables used in analysis extracted from Bering 10k simulation output; respiration (zooplankton) and remineralization (detrital) are distinct within the model but were summed to final total biological oxygen sinks.

Variable	Units
Oxygen	mmol O ₂ per m ³
Salinity	Practical Salinity Units (PSU)
Temperature	°C
Productivity	mg C per m ³ day
Respiration	mg C per m ³ day
Remineralization	mg C per m ³ day

Model Validation

Hindcast and future projection oxygen values were compared to observational values taken from regional cruises from 2008 to 2010. Model and observed points were matched by location, depth and date. They were plotted against one another and linear regressions were completed to determine the alignment between model and observed data. R and root mean square error were calculated for each scenario to show the degree of fit.

Analysis

Analysis focused on understanding and visualizing changes in bottom water oxygen on the Bering Sea shelf (bottom depth < 250 m) and drivers of oxygen. Three regions on the Bering shelf were examined: inner shelf (< 50 m depth), middle shelf (50-100 m depth), and outer shelf (100-250 m depth). Analysis was conducted for each individual shelf domain and for an average of the three shelf domains for each simulation.

Model output salinity and temperature values were used to calculate oxygen equilibrium solubility within the water column at all points (Equation 2) using empirical thermodynamic constants provided by Garcia and Gordon (1992). Bottom water temperature and salinity values were averaged across the Bering Sea shelf for each simulation, where temperature was in °C, salinity was in practical salinity units, and equilibrium solubility was in mmol O₂ per m³.

$$\text{Equilibrium Oxygen Solubility} = e^{A0_{O_2} + A1_{O_2} * T + A2_{O_2} * T^2 + A3_{O_2} * T^3 + A4_{O_2} * T^4 + A5_{O_2} * T^5 + S(B0_{O_2} + B1_{O_2} * T^2 + B3_{O_2} * T^3)} + C0_{O_2} * S^2 \quad (2)$$

Apparent oxygen utilization (AOU) was computed using equilibrium solubility values and model output oxygen value at every grid point in each given simulation (Equation 3). An AOU value equal to 0 would indicate that the dissolved oxygen equaled equilibrium solubility, while high values indicated that measured oxygen was much lower than the equilibrium solubility. AOU values below 0 can occur in shallow and stratified ocean during the summer when excess oxygen cannot be lost to the atmosphere or when water near the surface is warmed faster than the atmosphere.

$$\text{Apparent Oxygen Utilization} = \text{Equilibrium Oxygen Solubility} - \text{Model Oxygen} \quad (3)$$

All variables were averaged annually for each simulation and visualized through time series and spatial plots. Two-sided t-tests (significance level = 0.05) were calculated to compare

bottom-water oxygen values between initial (2011-2020 or 2031-2040) and final (2070-2079 or 2091-2100) decades for each future projection simulation. Percentage change in bottom oxygen value was also calculated between initial and final decades.

Monthly bottom water oxygen values were averaged across decades and used to visualize seasonal oxygen minimum values for each shelf domain. Frequency of bottom oxygen values below the threshold (140 $\mu\text{mol per m}^3$) was calculated. Seasonal bottom oxygen values were studied in the months September, October, and November (SON) as annual minimum oxygen values occurred during this period during both hindcast and forecast periods. Changes in the frequency (temporal and spatial) of values below these thresholds for the SON period were analyzed through time spatial plots.

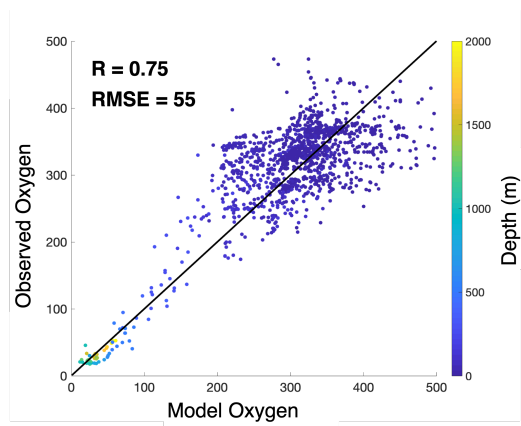
Biological processes (productivity, respiration and remineralization) were averaged annually at each grid point over the study period. These variables were depth-integrated at each point in the region to give an integrated water column value. Respiration (zooplankton) and remineralization (detrital) were summed as both are biological oxygen sinks. Depth integrated values of productivity and oxygen sinks were averaged on the Bering Sea shelf for each year. These were displayed through time series and spatial plots.

Results

Model Validation

Water column oxygen values were extracted from model output for the hindcast period. These values were matched with observed oxygen values corresponding to location and time. Matched points were plotted against each other to determine the fit of the model oxygen to observed data (Figure 1). The hindcast and observed values aligned strongly ($R = 0.75$; $RMSE = 55 \text{ mmol O}_2 \text{ per m}^3$) indicating that the Bering10k model was a useful tool for estimating oxygen values in the Bering Sea region. This analysis was replicated for each simulation to estimate skill for each version of the model. Bering10k simulations forced from CESM ($R = 0.76$; $RMSE = 64 \text{ mmol O}_2 \text{ per m}^3$) and GFDL ($R = 0.69$; $RMSE = 66 \text{ mmol O}_2 \text{ per m}^3$) showed strong correlation with observed data, while the MIROC simulations ($R = 0.46$; $RMSE = 125 \text{ mmol O}_2 \text{ per m}^3$) displayed less skill.

Figure 1: Correlation of bottom water oxygen ($\text{mmol O}_2 \text{ per m}^3$) values from Bering 10K hindcast and observations taken from 2008-2010 at points matched by location and depth; ($R=0.75$; $RMSE = 55$). Depth is represented by the colorbar; a one-to-one line is drawn to indicate a hypothetical perfect fit.

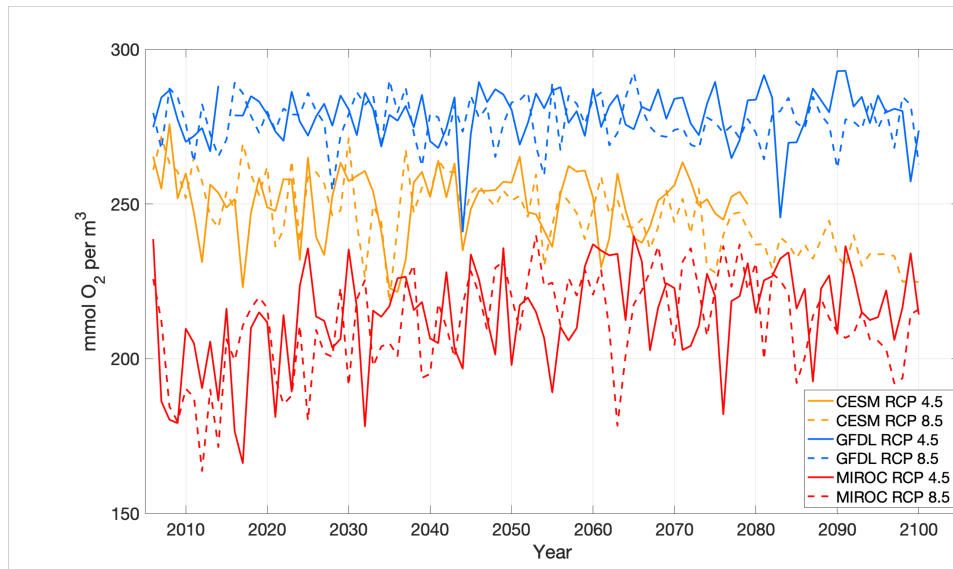


Simulation Data

Bottom water oxygen values were extracted and averaged annually over the Bering shelf (depth < 250 meters) for each of the 6 simulations (Figure 2). Bottom oxygen values varied

significantly for each of the three CMIP5 members reflecting biases of each. On average, the GFDL simulations for both RCP 4.5 and RCP 8.5 had the highest bottom oxygen values, and values were relatively constant with time over the 21st century. The CESM simulations showed a visible decline in bottom oxygen with time and simulated values. MIROC simulations showed the lowest average oxygen values in the majority of years, and bottom oxygen appeared to adjust until 2030 before stabilizing. All RCP 8.5 scenarios varied in regards to the corresponding RCP 4.5 simulation and generally showed stronger changes.

Figure 2: Bottom water oxygen values as a function of time on the Bering Sea shelf from simulations based on downscaled CMIP5 projections (CESM, GFDL-ESM2M, and MIROC at RCP 4.5 and 8.5) averaged annually across all points on the Bering Sea shelf (depth < 250 m).



Bottom oxygen values were compared from initial (2011-2020) to final (2091-2100) decades to determine the percent decline oxygen values (Table 2). A two-sided t-test (significance level = 0.05) was calculated between initial and final periods (null hypothesis: initial decade oxygen equals final decade oxygen values) and highlighted boxes show where the null hypothesis was rejected. The null hypothesis is rejected for both CESM simulations. In both CESM simulations, there was a significant decline in bottom oxygen and middle shelves, while

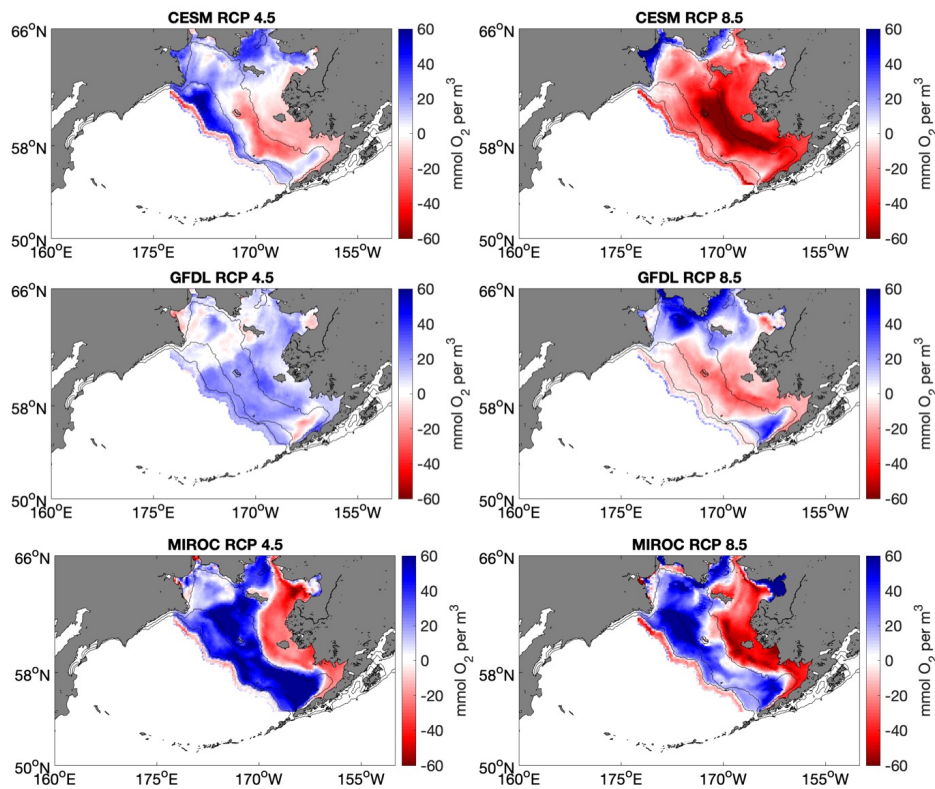
bottom oxygen decreases on all shelves at RCP 8.5. GFDL simulations showed percentage changes close to zero, with no significant changes between initial and final decades (null hypothesis was not rejected). Both MIROC simulations show significant increase in the middle and outer shelves, while the inner shelf significantly declines at RCP 8.5.

Table 2: The percentage change in bottom water oxygen values on the Bering Sea shelf (depth < 250 m) based on initial (2011-2020) and final (2091-2100) decades; entries are highlighted based on significance of change (p-value < 0.05). Red shows significant decline in bottom water oxygen; blue shows significant increase in bottom water oxygen.

	CESM		GFDL		MIROC	
	4.5	8.5	4.5	8.5	4.5	8.5
Inner	-1.19%	-8.87%	0.52%	-0.42%	-2.90%	-7.24%
Middle	-3.34%	-14.30%	-0.85%	1.36%	17.90%	16.00%
Outer	3.85%	-12.20%	2.96%	0.62%	20.44%	23.77%

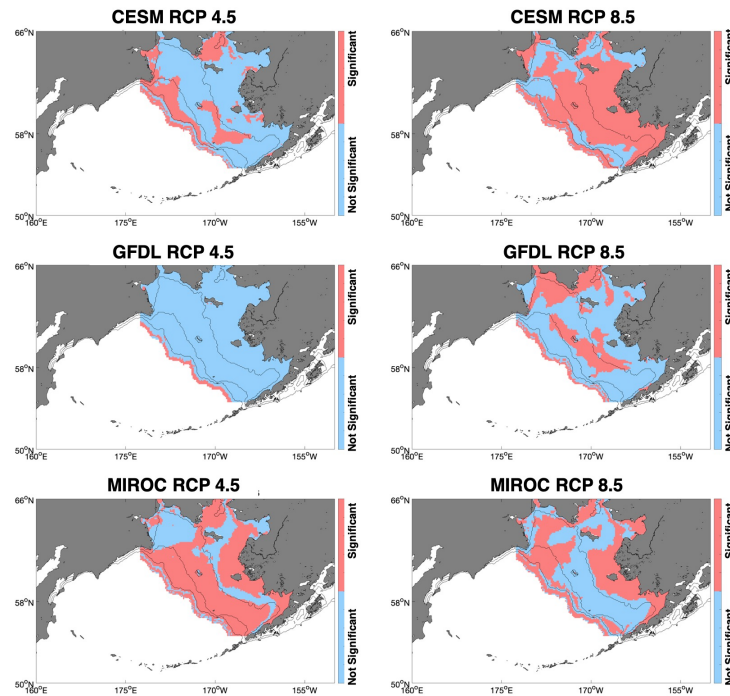
Each grid point was averaged over initial (2011-2020) and final decade (2091-2100) periods for bottom oxygen. Spatial values were then differenced to find the change in bottom oxygen over the century (Figure 3). The CESM simulations showed a clear change between the RCP scenarios, with RCP 8.5 exhibiting a wider region covered by red (corresponding to oxygen decline) as compared to the RCP 4.5 scenario. This corresponds to Tables 1 and 2 above, which showed significant declines in bottom oxygen across the shelf region in CESM for RCP 8.5. The two GFDL simulations were relatively distinct spatially, as regions with projected increases in oxygen in the RCP 4.5 scenario have declines in the RCP 8.5 scenario. In both MIROC scenarios, the inner shelf showed strong oxygen declines, while the middle and outer shelves oxygen values increased. All simulations supported increasingly significant change under high emission scenarios.

Figure 3: Difference in bottom oxygen from initial (2011-2020) to final (2091-2100) decades on Bering Sea shelf (depth < 250 m) for all simulations. Negative values (red) indicate a decrease in oxygen over the century.



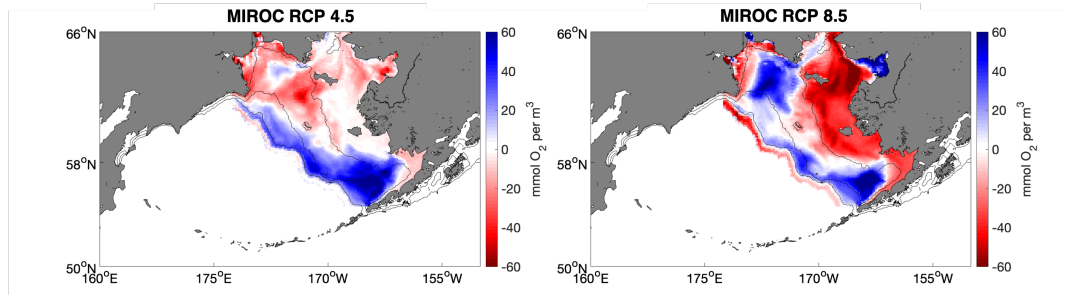
The significance of changes in annual bottom water oxygen values from initial to final decades was displayed spatially on the Bering Sea shelf for each simulation based on the results of a two-sided t-test (Figure 4). CESM showed larger areas of significant change in the RCP 8.5 scenario. GFDL showed some oxygen decline spatially for RCP 8.5, but a large portion of the shelf showed no significant differences. MIROC scenarios showed larger portions of significant difference for RCP 4.5, but both RCP 4.5 and 8.5 showed large regions with significant differences between decades.

Figure 4: Spatial map of significant changes in bottom water oxygen values changes for each simulation according to a two-sided t-test for significance (p -values < 0.05). Light red values show significant change, light blue values show insignificant changes.



Due to the adjustment (decline followed by a partial rebound) observed in MIROC simulations (shown in Figure 2), another baseline decade (2031-2040) was also used in analysis of decadal differences for both MIROC simulations (Figure 5). MIROC at RCP 4.5 showed declining bottom oxygen on the inner shelf, but an increase on the outer shelf region. MIROC at RCP 8.5 showed a decline of bottom oxygen on the inner shelf and some increase on the middle and outer shelves. Two-sided t-tests were conducted to compare decadal values on each shelf region. Significance ($p < 0.05$) was only found to occur within MIROC on the outer shelf region (significant increase in oxygen) at RCP 4.5 and on the inner shelf (significant decline in oxygen) at RCP 8.5. This differs from the more significant change observed using the 2011-2020 period as a baseline.

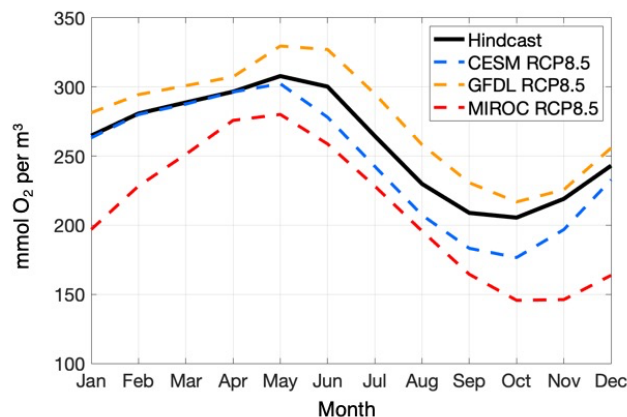
Figure 5: Difference in bottom oxygen from initial (2031-2020) to final (2091-2100) decades on Bering Sea shelf (depth < 250 m) for MIROC simulations. Negative values (red) indicate a decrease in oxygen over the century.



Seasonal Oxygen Cycling

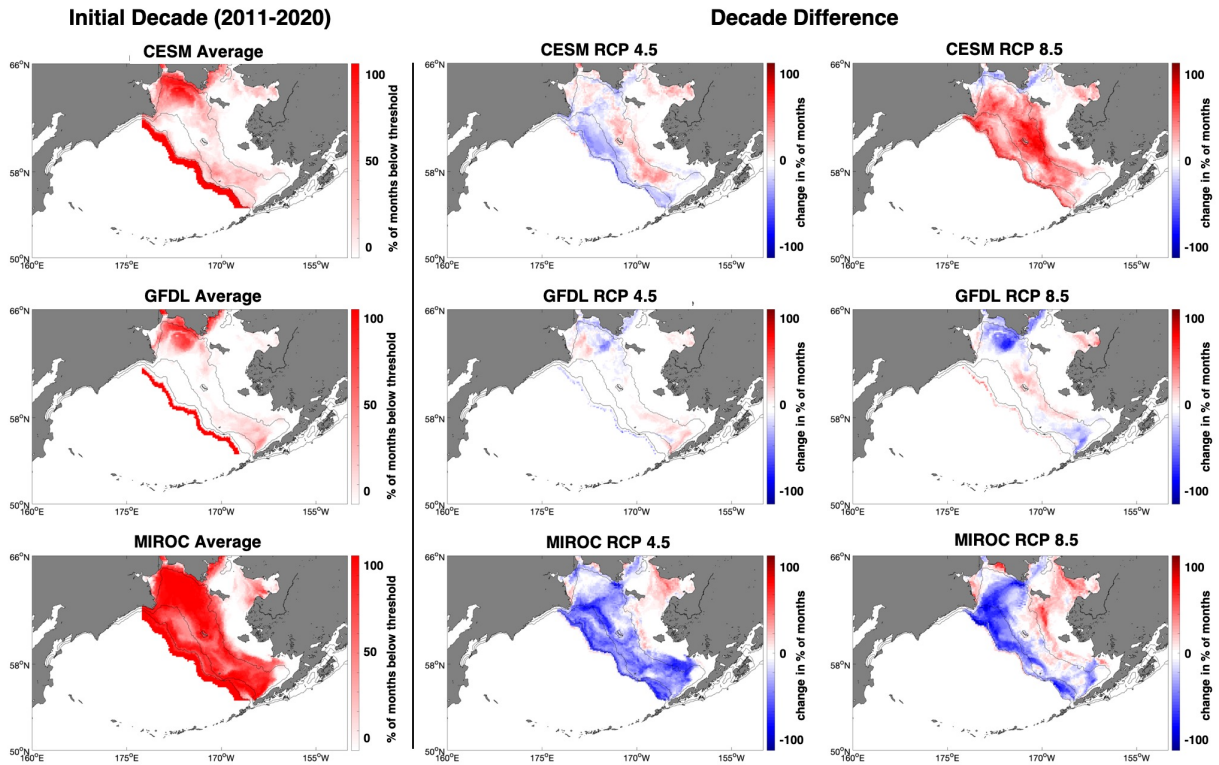
Analysis of seasonal bottom oxygen values showed that the annual minimum tended to occur in the period of September to November across simulations (Figure 6). The simulated seasonal cycles and oxygen minima were consistent in both the hindcast and the high-end (RCP 8.5) simulations with distinctive seasonal low values in these months. Changes in seasonal low oxygen zones across the 21st century focused on these months (September, October, and November; SON).

Figure 6: Seasonal cycling of bottom water oxygen averaged over all years in the hindcast (2003-2012) and forecast periods (2006-2100) at RCP 8.5. Values peaked in late spring months and exhibited a trough in fall months.



The percent of time for Fall months (SON) with average bottom oxygen below the threshold was calculated for both the initial (2011-2020) and final (2091-2100) decades. The initial decade percent values (averaged for each of: CESM, GFDL, MIROC) and change between final and initial decades (for each simulation) were plotted spatially (Figure 7). The first column showed the percent of months (SON) in the initial decade below the threshold. CESM and GFDL showed similar spatial patterns, with a high percentage of months below the threshold on the edge of the Bering Sea shelf. MIROC showed a high percentage below the threshold on both the middle and outer shelves in the initial period. The second and third columns showed change in percentage of months below the threshold from initial to final decade. CESM for both RCP 4.5 and 8.5 showed an increase in the percentage of months below the threshold over the period. GFDL simulations did not show a clear change over the decadal period. MIROC at RCP 4.5 and RCP 8.5 showed an increase in values on the inner shelf and decrease in percentage on the outer shelf (similar to changes observed in average annual bottom oxygen values).

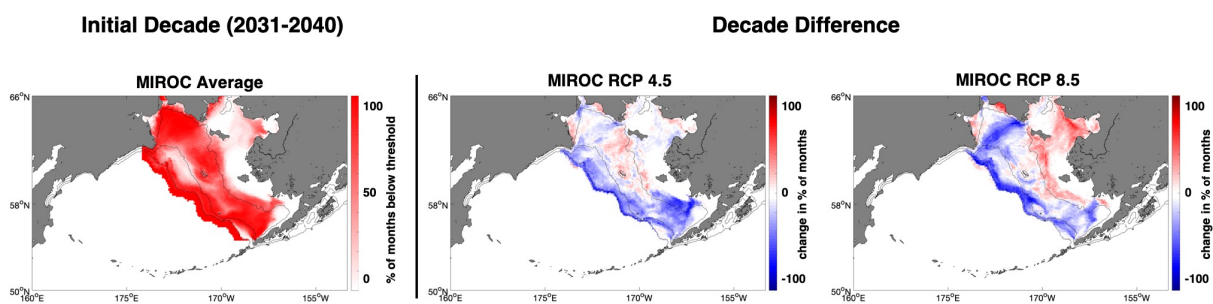
Figure 7: The percent of time bottom water oxygen in Fall (months of SON) was below the threshold ($140 \text{ mmol O}_2 \text{ per m}^3$) in the initial (2011-2020) decade averaged across CMIP5 ensemble member (left column); change in percent time below the threshold between initial (2011-2020) and final (2091-2100) decades. Positive increase (red values) indicate an increase in the amount of time below the threshold in the final decade.



Due to the large initial adjustment (decline followed by a partial rebound) observed in MIROC simulations, another baseline decade (2031-2040) was also used in analysis of seasonal differences (as for decadal differences in Figure 5) (Figure 8). The percentage of time during Fall months (SON) below the oxygen threshold was calculated for both the initial and final decadal periods. The initial decade (left column) in MIROC showed a large spatial area with high percentage of time below the threshold. The change in percentage of time below the threshold from initial to final decade is displayed (right columns). Over the century, there are both regional increases and decreases in percent of area below the threshold. Both RCP scenarios suggest an

increase in low oxygen on the inner shelf, and a decline in percentage of time below the threshold on the middle and outer shelves.

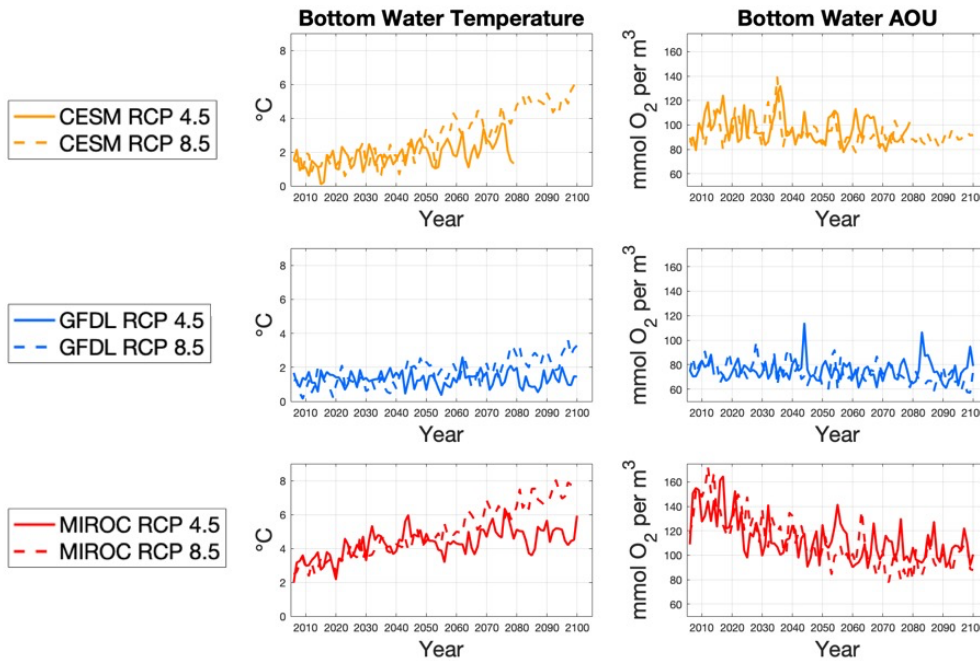
Figure 8: The percent of time bottom water oxygen in SON was below the threshold (140 mmol O₂ per m³) in the initial (2011-2020) decade averaged across MIROC (left column). Change in percent of time (SON) below the threshold between initial (2031-2040) and final (2091-2100) decades. Positive increase (red values) indicate an increase in the percent of time below the threshold in the final decade.



Oxygen Drivers

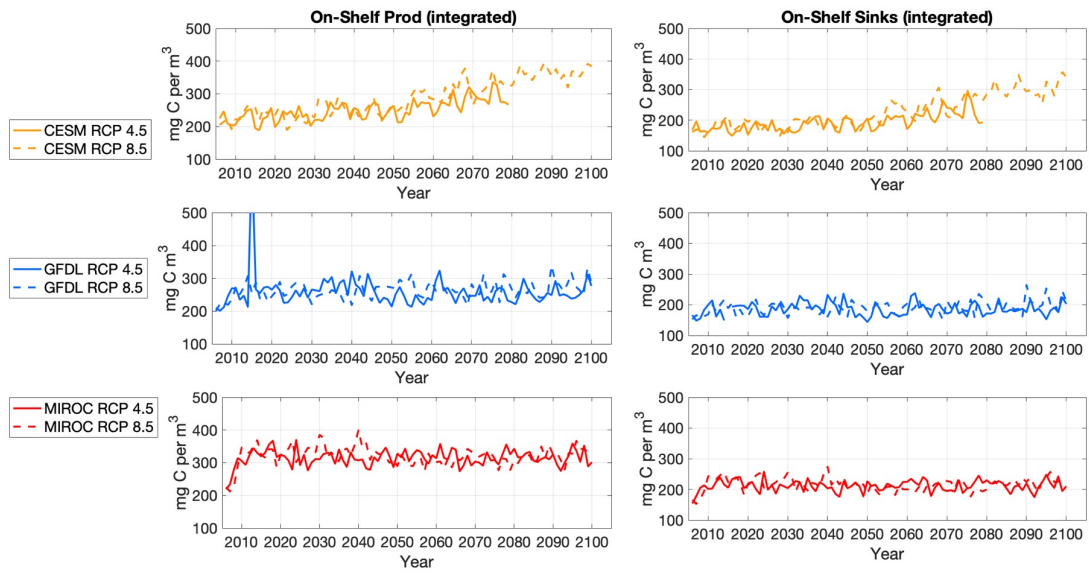
For the Bering 10k simulations, changes in simulated bottom oxygen are driven by changes in physical features (oxygen solubility, AOU) and biological processes. Century-long time series for bottom water temperature and AOU were displayed (Figure 9). Changes in solubility were estimated using the century-long trends in temperature and AOU estimated changes in biological processes. Increases in temperature were larger for high warming scenarios (RCP 8.5) than for moderate warming scenarios (RCP 4.5). On average, there was a warming of bottom waters by $\sim 2.2^{\circ}\text{C}$ across all scenarios, with the highest warming signal in MIROC at RCP8.5 ($\sim 5^{\circ}\text{C}$) and lowest in GFDL at RCP 4.5 ($\sim 0.1^{\circ}\text{C}$). Over the study period AOU was generally observed to decline. There was a 59% decline in apparent oxygen utilization averaged across all scenarios. The declining trend was strongest in MIROC (-54%) simulations, followed by GFDL (-13%) and CESM (-11%) simulations.

Figure 9: Time series showing century-long changes in bottom water temperature ($^{\circ}\text{C}$) and apparent oxygen utilization (mmol O_2 per m^3) averaged across all shelves for all simulations.



Biological processes were averaged across Bering Sea shelf region and depth-integrated for each simulation (Figure 10). All simulations showed increases in depth-integrated productivity and oxygen sinks (respiration + remineralization). Both CESM scenarios showed strong increases from initial to final decades that were statistically significant (according to a two-sided t-test) in productivity (20% and 34% respectively) and oxygen sinks (21% and 41% respectively). GFDL showed similar trends, with stronger increases coming in RCP 8.5 scenarios in productivity (13%) and oxygen sinks (13%) from initial to final decades. MIROC simulations showed strongest increases at RCP 8.5 scenarios in productivity (10%) and oxygen sinks (16%).

Figure 10: Biological processes affecting oxygen values integrated across all depths. Productivity is a source of oxygen, while sinks (respiration + remineralization) lower oxygen values.



Discussion

The global ocean is experiencing significant temperature rise, acidification, and deoxygenation due to global climate change. This study focused on estimating and simulating changes in bottom water oxygen in the Bering Sea under various climate scenarios. It was expected that the Bering Sea would display significant oxygen declines and increases in the frequency of values below biologically-significant oxygen thresholds. As expected, the response of bottom oxygen values varied depending on both the source of the climate and boundary conditions (CESM, GFDL, MIROC) and emissions scenarios (RCP 4.5 and 8.5). Differing climate models project different levels of global climate change for the same RCP scenarios, and these differences are especially strong at the regional scale. Bottom oxygen was shown to decrease over the 21st century over large regions of the shelf for two of the models, corresponding to an increase in frequency and spatial extent of seasonal oxygen minimum zones.

Although the three climate models used here capture some of the model-to-model differences within the CMIP5 ensemble projections, they span only a portion of the large model ensemble variance. The computational expense of dynamically downscaled models limits the quantity of ensemble members that can be used. Model drift associated with different climate model forcing within the general Bering10k simulation was not analyzed as a part of this study, which may have led to internal biases and inconsistencies within output data over the 21st century study period. This may be particularly true for the MIROC simulations, which exhibited a large early adjustment period away from hindcast model conditions. Regional and global effects of advection on biogeochemical signals at lateral boundary conditions were also ignored within this analysis. Ocean biological processes exhibit strong vertical patterns (e.g. difference in biogeochemical cycling between photic and aphotic zones) and this study did not measure export

production and organic carbon fluxes across the boundary between the photic and aphotic zone, one area for future exploration of oxygen in the region. Stratification of the water column due to changing water temperature is a major driver of global deoxygenation and was not quantified in this study.

Scenario-Specific Change

The GFDL model was expected to show the weakest changes in bottom oxygen values as it had the lowest regional warming signal values of the chosen CMIP5 ensemble members. Results showed that GFDL simulations experienced moderate change in bottom oxygen. No significant changes between initial and final decadal values were noted for seasonal thresholds or biological processes over the 21st century.

MIROC had the highest warming trend of any of the CMIP5 members forcing the Bering10k, so a strong decline in regional bottom oxygen was expected. The hypothesis was rejected for MIROC simulations using the initial decade 2011-2020, as simulations showed strong increases in oxygen values in both the middle and outer shelf regions cancelling out inner-shelf declines. Due to the high initial variability in MIROC simulations (likely caused by model adjustment and not reflecting a climate change signal) a second initial decade (2031-2040) was used for analysis.

Oxygen was observed to decline on the inner shelf and increase on the middle and outer shelves in analysis using both initial decades. The later initial decade showed less significant change. Seasonally, MIROC showed an increase in months below the threshold on the inner shelf over the study period using both 2011-2020 and 2031-2040 baselines. Both initial decades analyzed showed a large percentage of bottom oxygen values below the threshold on the middle and outer shelves, and changes over the century are negligible on those shelves. More work is

needed to understand the processes contributing to this unexpected increase in bottom oxygen in middle and outer shelf regions. Strong variations in bottom oxygen relative to CESM and GFDL may be explained by low model skill and bias ($R = 0.46$; $RMSE = 125$) although no identified feature explained the increase in bottom oxygen on middle and outer shelf regions.

The CESM simulation was closest to the average warming shown in the CMIP5 ensemble in the Bering Sea region (Herman et al. 2019). Oxygen values were expected to decline a moderate amount as compared to GFDL (low warming) and MIROC (high warming). The hypothesis of oxygen decline was supported for the CESM simulation. The simulations for RCP 4.5 showed significant decline on the middle shelf, while RCP 8.5 showed significant declines on all shelf domains. Spatial plots show that RCP 8.5 scenario leads to a strong region-wide decline in oxygen values, corresponding to an increase in the percentage of the SON period with oxygen values below the threshold from initial to final decades. Model skill as compared to observational data was highest for CESM.

Full attribution of changes in oxygen to specific variables was not completed in this analysis, but using CESM as an example, it was possible to estimate the effects of these drivers. Shelf-wide bottom oxygen was changed by an average of -0.8 mmol O_2 per m^3 (RCP 4.5) and -14 mmol O_2 per m^3 (RCP 8.5). Bottom temperatures in the simulations increased by $1.4^\circ C$ (RCP 4.5) and $3.7^\circ C$ (RCP 8.5) on the Bering Sea shelf, lowering shelf-wide oxygen solubility by 6.6 mmol O_2 per m^3 (RCP 4.5) and by 26 mmol O_2 per m^3 (RCP 8.5). AOU also declined by 13 mmol O_2 per m^3 (RCP 4.5) and 13 mmol O_2 per m^3 (RCP 8.5) over the century, likely driven by changes in ventilation. The similarity of AOU values for each RCP scenario was probably due to model spin-up issues or a threshold effect.

Oxygen sinks and productivity increased in both scenarios. Depth-integrated oxygen sinks increased by a larger percentage than the depth-integrated productivity, especially at RCP 8.5. This might have led to a potential imbalance in oxygen sinks (biological sinks > sources) that could have driven oxygen declines. Declines in both bottom oxygen and solubility increased in scale from scenarios RCP 4.5 to 8.5, while change in AOU remained constant for both emission scenarios. As noted in equation 2, AOU was equal to the difference of equilibrium solubility and model output oxygen. Using the changes in AOU and solubility values over the study period to estimate changes in bottom oxygen was a success, as values were equal for both RCP scenarios. This suggested that changes in bottom oxygen may have been related primarily to changes in solubility. Increase in respiration rates combined with temperature-driven declines in oxygen solubility could explain the majority of the annual bottom oxygen decline observed within CESM simulations.

Seasonal Oxygen Declines

While concentrated regions of true hypoxic water (below ~ 65 mmol per m^3) were not observed in any of the simulations, increases in the occurrence of seasonal and regional values below a general fish stress threshold (~ 140 mmol per m^3) were widely observed, especially on the middle shelf region. Both initial decade periods analyzed for MIROC simulations showed large regions under the threshold. Changes by the end of the century within CESM simulations also showed a large increase in spatial extent below this threshold. More work is needed to estimate when these oxygen minimum zones will reach a duration and scale that may affect commercial fish stocks in the region. Testing to determine oxygen behavioral and mortality thresholds of specific commercially-important fish in the region (pollock, cod, haddock, halibut,

crabs, etc.) could also prove useful in determining the threat to Bering Sea fisheries posed by regional deoxygenation as these species likely have variable oxygen requirements.

Summary

Bottom oxygen in the Bering Sea significantly decline across the 21st century in some simulations (CESM), increased and decreased regionally (MIROC), and showed no significant trend in others (GFDL). Changes reflect alterations in ocean physical and biological process driven by climate change. According to best estimates (CESM), bottom oxygen can be expected to be significantly lower across large regions of the Bering Sea shelf and seasonal oxygen minimum will occur with increasing frequency by the end of the century, likely threatening commercially-important fish. Future work studying oxygen in the region should focus on identifying regionalized drivers of oxygen trends on all shelves and in all simulations. The effects of changes in temperature and biological processes need to be more quantitatively correlated to changes in bottom oxygen values.

References

- Bopp, L., L. Resplandy, J. C. Orr, S. C. Doney, J. P. Dunne, M. Gehlen, P. Halloran, et al. 2013. “Multiple Stressors of Ocean Ecosystems in the 21st Century: Projections with CMIP5 Models.” *Biogeosciences* 10 (10): 6225–45. <https://doi.org/10.5194/bg-10-6225-2013>.
- Breitburg, Denise, Lisa A. Levin, Andreas Oschlies, Marilaure Grégoire, Francisco P. Chavez, Daniel J. Conley, Véronique Garçon, et al. 2018. “Declining Oxygen in the Global Ocean and Coastal Waters.” *Science* 359 (6371): eaam7240. <https://doi.org/10.1126/science.aam7240>.
- Deutsch, C., A. Ferrel, B. Seibel, H.-O. Portner, and R. B. Huey. 2015. “Climate Change Tightens a Metabolic Constraint on Marine Habitats.” *Science* 348 (6239): 1132–35. <https://doi.org/10.1126/science.aaa1605>.
- Doney, Scott C., Victoria J. Fabry, Richard A. Feely, and Joan A. Kleypas. 2009. “Ocean Acidification: The Other CO₂ Problem.” *Annual Review of Marine Science* 1 (1): 169–92. <https://doi.org/10.1146/annurev.marine.010908.163834>.
- Feely, Richard A, Scot T C Doney, and Sar Ah R Cooley. 2020. “Ocean Acidification,” 13.
- Hameau, Angélique, Thomas L. Frölicher, Juliette Mignot, and Fortunat Joos. 2020. “Is Deoxygenation Detectable before Warming in the Thermocline?” *Biogeosciences* 17 (7): 1877–95. <https://doi.org/10.5194/bg-17-1877-2020>.
- Hermann, Albert J., Georgina A. Gibson, Nicholas A. Bond, Enrique N. Curchitser, Kate Hedstrom, Wei Cheng, Muyin Wang, Edward D. Cokelet, Phyllis J. Stabeno, and Kerim Aydin. 2016. “Projected Future Biophysical States of the Bering Sea.” *Deep Sea Research Part II: Topical Studies in Oceanography* 134 (December): 30–47. <https://doi.org/10.1016/j.dsr2.2015.11.001>.
- Hermann, Albert J, Georgina A Gibson, Wei Cheng, Ivonne Ortiz, Kerim Aydin, Muyin Wang, Anne B Hollowed, and Kirstin K Holsman. 2019. “Projected Biophysical Conditions of the Bering Sea to 2100 under Multiple Emission Scenarios.” Edited by Shubha Sathyendranath. *ICES Journal of Marine Science*, April, fsz043. <https://doi.org/10.1093/icesjms/fsz043>.
- Ito, Takamitsu, Shoshiro Minobe, Matthew C. Long, and Curtis Deutsch. 2017. “Upper Ocean O₂ Trends: 1958-2015: OXYGEN TRENDS.” *Geophysical Research Letters* 44 (9): 4214–23. <https://doi.org/10.1002/2017GL073613>.
- Khatiwala, S., F. Primeau, and T. Hall. 2009. “Reconstruction of the History of Anthropogenic CO₂ Concentrations in the Ocean.” *Nature* 462 (7271): 346–49. <https://doi.org/10.1038/nature08526>.
- Kwiatkowski, Lester, Olivier Torres, Laurent Bopp, Olivier Aumont, Matthew Chamberlain, James Christian, John P. Dunne, et al. 2020. “Twenty-First Century Ocean Warming, Acidification, Deoxygenation, and Upper Ocean Nutrient Decline from CMIP6 Model Projections.” Preprint. Earth System Science/Response to Global Change: Models, Holocene/Anthropocene. <https://doi.org/10.5194/bg-2020-16>.
- Laffoley, D., and J.M. Baxter, eds. 2019. *Ocean Deoxygenation: Everyone’s Problem. Causes, Impacts, Consequences and Solutions*. IUCN, International Union for Conservation of Nature. <https://doi.org/10.2305/IUCN.CH.2019.13.en>.

- Oschlies, Andreas, Peter Brandt, Lothar Stramma, and Sunke Schmidtke. 2018. "Drivers and Mechanisms of Ocean Deoxygenation." *Nature Geoscience* 11 (7): 467–73.
<https://doi.org/10.1038/s41561-018-0152-2>.
- Panteleev, Gleb, Vladimir Luchin, Nikolay P. Nezlin, and Takashi Kikuchi. 2013. "Seasonal Climatologies of Oxygen and Phosphates in the Bering Sea Reconstructed by Variational Data Assimilation Approach." *Polar Science* 7 (3–4): 214–32.
<https://doi.org/10.1016/j.polar.2013.10.001>.
- Pilcher, Darren J., Danielle M. Naiman, Jessica N. Cross, Albert J. Hermann, Samantha A. Siedlecki, Georgina A. Gibson, and Jeremy T. Mathis. 2019. "Modeled Effect of Coastal Biogeochemical Processes, Climate Variability, and Ocean Acidification on Aragonite Saturation State in the Bering Sea." *Frontiers in Marine Science* 5 (January): 508.
<https://doi.org/10.3389/fmars.2018.00508>.
- Siedlecki, S. A., N. S. Banas, K. A. Davis, S. Giddings, B. M. Hickey, P. MacCready, T. Connolly, and S. Geier. 2015. "Seasonal and Interannual Oxygen Variability on the Washington and Oregon Continental Shelves." *Journal of Geophysical Research: Oceans* 120 (2): 608–33. <https://doi.org/10.1002/2014JC010254>.
- Talley, L.D. 2007. "Hydrographic Atlas of the World Ocean Circulation Experiment (WOCE)." *Volume 2: Pacific Ocean* (eds. M. Sparrow, P. Chapman and J. Gould).
<https://doi.org/10.21976/C6WC77>
- Vaquier-Sunyer, Raquel, and Carlos M. Duarte. 2008. "Thresholds of Hypoxia for Marine Biodiversity." *Proceedings of the National Academy of Sciences* 105 (40): 15452–57.
<https://doi.org/10.1073/pnas.0803833105>.